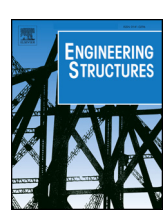
FISEVIER

Contents lists available at ScienceDirect

## **Engineering Structures**

journal homepage: www.elsevier.com/locate/engstruct



# Equivalent viscous damping for a system with energy dissipation via elastic instabilities



Mansour Alturki<sup>a</sup>, Rigoberto Burgueño<sup>b,\*</sup>

- <sup>a</sup> Department of Civil Engineering, College of Engineering, Qassim University, Buraydah 51452, Saudi Arabia
- b Department of Civil Engineering, 2430 Computer Science, Stony Brook University, Stony Brook, NY 11794-4424, United States

#### ABSTRACT

This paper presents a study to investigate the equivalent viscous damping (EVD) for the hysteretic response of a multiple cosine-curved dome (MCCD) system. The system comprises of several serially connected units with elastic multistable behavior. The system relies on consecutive snap-through buckling events of the connected units to elastically dissipate energy. The study aims to facilitate the direct displacement-based design of structures incorporating such systems as the main damping mechanism to dissipate seismic energy. Time-history analyses of linear and nonlinear single degree of freedom systems were performed to compare spectral displacements and EVD ratios of the hysteretic response of MCCD systems to their substitute linear systems in terms of maximum displacements. A set of 62 ground motion records were considered for the analysis. A statistical study was conducted on the resulting displacements and the EVD ratios to develop expressions for EVD ratios of the hysteretic response. Results show that using proposed EVD ratios for the substitute linear systems yields good approximations for the peak spectral displacements compared to the original nonlinear systems.

## 1. Introduction

Recent developments in innovative discrete systems composed of elements with elastic instabilities have facilitated the potential of using such systems for energy dissipation and shock absorption applications [1-9]. These systems offer recoverable elastic deformations with a significant hysteretic response. One potential application of discrete systems is as damping elements in structures resisting seismic actions as shown in Fig. 1. The figure shows examples of structural systems equipped with supplementary energy dissipation devices comprised of chains of elastic multistable elements. The possibility of using such elements for seismic protection enables avoiding typical shortcomings of commonly used passive hysteresis energy dissipation devices. For example, a typical issue with metallic devices is that they require repair or replacement after a strong seismic action due to damage [10]. An issue with friction-based devices is that they significantly increase the initial stiffness and strength of the structure, which in turn increases force demands on other members of the structure that should remain elastic [11].

This work introduces the use of hysteretic response from a discrete system composed of multistable cosine-curved domes [12] to seismic loading and design by investigating the equivalent viscous damping (EVD) and considering the unique response characteristics of the system compared to commonly used inelastic hysteresis models. The uniqueness of elastic multistable element systems originates from the fact that

their response cannot be directly described by the displacement ductility or apparent displacement ductility, which is a commonly used measure for energy dissipation. Instead, the response is characterized by the number of units in a system and their response, which control the amount of dissipated energy. Understanding this fundamental difference is the key to properly designing such systems as the main damping mechanism in structures. The work herein is based on this conceptual difference.

Accurate estimations for the EVD ratios is an essential step to the direct displacement-based design, as this quantity relates the hysteretic response of a structure to its corresponding spectral displacement for a given ground motion record. Methods used to investigate the EVD involve conducting dynamic analyses on linear and nonlinear systems. In this study, time-history analyses (THA) were performed on the hysteretic response of discrete systems and their substitute linear systems in terms of maximum displacements to study the ratio of nonlinear to linear displacements. This was followed by an iterative THA procedure to determine EVD ratios for the equivalent substitute linear systems. A statistical study was then conducted on the results to develop expressions for EVD ratios of the hysteretic response.

## 1.1. System with hysteretic response from elastic instability

The examined system in this study is a multistable cosine-curved dome (MCCD) system, details of which are presented in reference [12].

E-mail addresses: m.alturki@qu.edu.sa (M. Alturki), Rigoberto.Burgueno@stonybrook.edu (R. Burgueño).

<sup>\*</sup> Corresponding author.

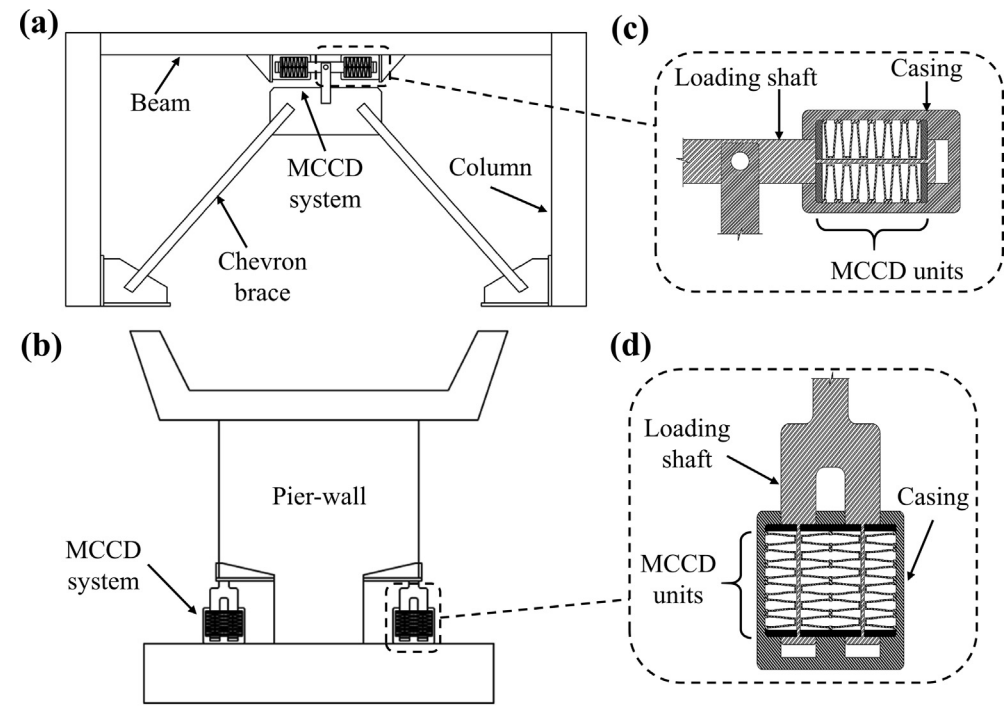


Fig. 1. Example applications of the MCCD system incorporated in typical structural systems: (a) frame with a chevron brace, (b) pier-wall, (c) single-column, and (d) double-column MCCD systems.

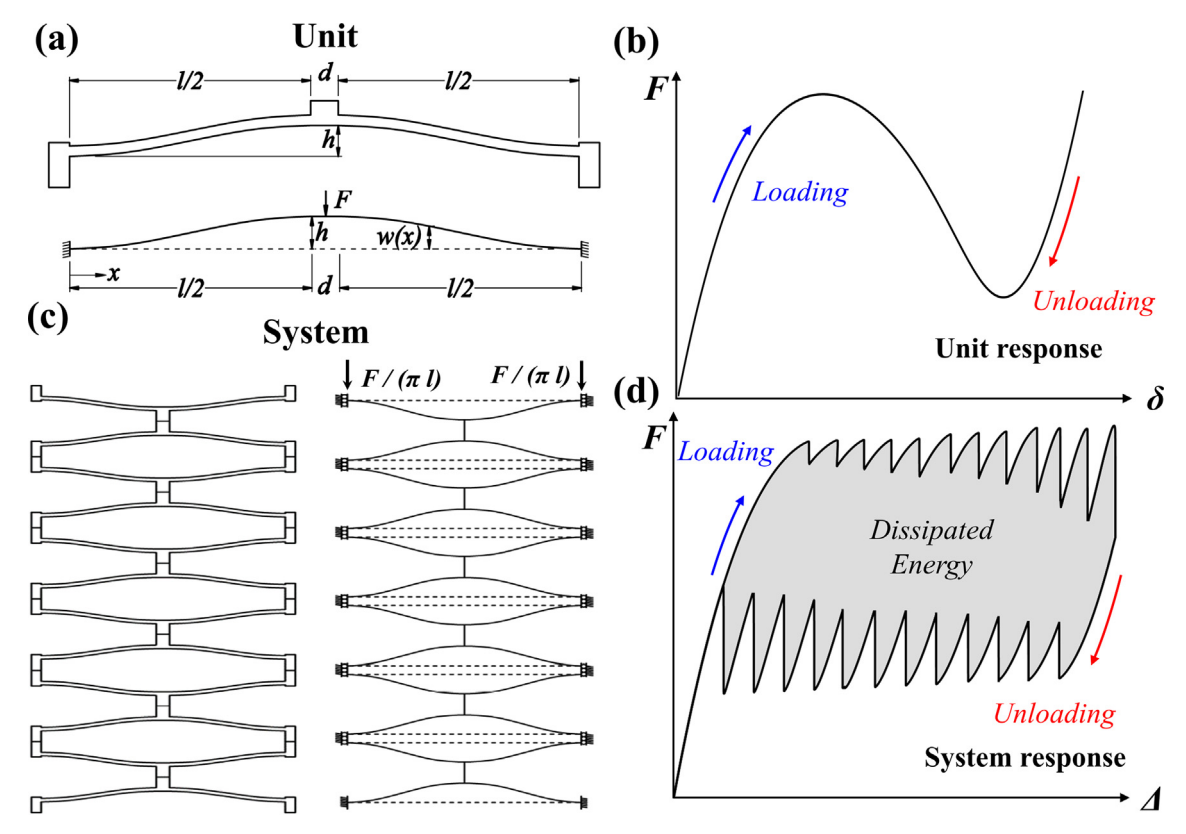


Fig. 2. The considered system: (a) cross-section of a single unit, (b) schematic force—displacement response of a single unit, (c) MCCD system composed of multiple units, and (d) schematic hysteretic response of the MCCD system.

The system is comprised of several cosine-curved dome units [13] with geometric properties as shown in Fig. 2(a). The units are linked in series as shown in Fig. 2(c). The individual units exhibit a tailorable elastic limit-point response (snap-through instability) with a negative stiffness region as shown in Fig. 2(b). If a sufficient number of serially connected

units is used, the MCCD system will exhibit a response with multiple snap-through buckling events and distinct loading and unloading paths that lead to an elastic hysteretic response with self-centering capability as shown in Fig. 2(d). The characteristics of this response mainly depends on the number of connected units,  $n_s$ , in the system and on the

height-to-thickness ratio, h/t, of the repeated units. The higher the values of h/t and  $n_s$ , the larger the hysteresis loop.

The area enclosed by the loading and unloading paths represents the elastically dissipated energy. The energy dissipation in such elastic systems is due to the transformation of some of the induced mechanical energy of the applied work into elastic vibrations that are damped by the base material of the repeating units and converted to irreversible thermal energy (heat) with each snap-through event. These elastic vibrations occur when the deforming system has at least 3 or more elements connected in series to allow relative movement of the units at a given system displacement of a snapping event. Increasing the number of linked elements in series has two effects on the response of the system: (a) it increases the number of vibrating elements in the system, and (b) it increases the number of events of system disturbances that cause vibrations.

## 1.2. Direct displacement-based design

An ideal method to design structures with energy dissipation devices is the direct displacement-based design (DDBD) method [14,15] since it based on the deformation of the structure rather than its strength. Therefore, this method relies on displacement demands and modified linear elastic displacement spectra for design. To understand the work presented here, it is important to first to recall the main steps of the DDBD method, which are given below with reference to Fig. 3 (where  $\Delta_y$  and  $F_y$  are the apparent yield displacement and force at yield, respectively,  $\Delta_u$  and  $F_u$  are the ultimate displacement and force, respectively,  $\mu_\Delta$  is the displacement ductility,  $k_i$  and  $k_t$  are the initial and tangent stiffnesses, respectively,  $k_{eff}$  is the effective stiffness at the point of maximum displacement, and  $S_d$  is the spectral displacement demand):

- 1. Determine the design (ultimate) displacement,  $\Delta_u$ . Usually, this displacement is based on maximum allowable drift limits or on sectional/element deformation limits [Fig. 3(a)].
- 2. Determine the yield (ideal) displacement,  $\Delta_y$ . This displacement is usually based on the target displacement ductility level,  $\mu_{\Delta}$ , serviceability drift limits, or on sectional/element deformation limits [Fig. 3(a)].
- 3. Based on the displacement ductility, determine the EVD ratio,  $\xi$ , for the proper model of the hysteretic response [Fig. 3(b)]. Several expressions to estimate  $\xi$  for various hysteresis models are available in the literature [16–22]. These expressions are usually in terms of  $\mu_{\Delta}$ , the structural period, T, and other parameters of the hysteresis model.
- 4. Using  $\xi$  and the design displacement, determine the effective

- structural period,  $T_{eff}$ , from the modified displacement response spectrum [Fig. 3(c)].
- 5. Calculate the effective stiffness,  $k_{eff}$ , and hence the design force,  $F_u$ , at the ultimate displacement [Fig. 3(a)].

The key step from the DDBD procedure that this study focuses on is the third step, since it links the response of the hysteretic model and the ductility level of the element under consideration to the EVD. The value of  $\xi$  is then used to modify the design linear elastic displacement response spectrum. This eliminates the need to conduct nonlinear THA to obtain nonlinear displacement response spectra for the design process. Therefore, the DDBD method requires an accurate estimation of  $\xi$  for a substitute linear single degree of freedom (SDF) system that represents, in terms of maximum spectral displacement, the response of the actual nonlinear system for design purposes as shown in Fig. 3, which consequently eliminates the need to perform THA for the system.

## 1.3. Approaches to estimate equivalent viscous damping ratio

The equivalent viscous damping ratio ( $\xi$ ) can be divided into two parts: (a) the initial or elastic viscous damping ratio,  $\xi_e$ , and (b) the hysteresis damping ratio,  $\xi_h$ , as given in Eq. (1). The elastic viscous damping is the damping inherited by the materials of the structure and proportional to the loading rate (velocity). This type of damping usually ranges between 2 and 7% for common structural materials and elements [23–25]. The hysteresis damping is the resulting damping from energy dissipation by the hysteretic response of the system. This damping is significantly higher than the elastic damping.

$$\xi = \xi_e + \xi_h \tag{1}$$

Unfortunately, there is no direct procedure to estimate  $\xi$  for a given hysteresis model since the available direct approaches to determine this quantity, such as Jacobsen's approach [26,27], are affected by many factors, including the forcing function on the SDF system and the structural period shift. Thus, such a method cannot be directly applied for nonlinear systems excited by ground motion records with nonuniform frequency content. Proper estimations for  $\xi$  are therefore usually achieved by analyzing nonlinear SDFs and their linear equivalents under a wide range of ground motion records. Studies in [16–22] showed that the resulting equivalent damping ratio for SDFs under ground motion records is lower than that determined using Jacobsen's approach.

There are two main approaches followed to estimate the maximum displacement of a nonlinear hysteretic system from its substitute linear system in order to develop design expressions [28]. In the first approach, the maximum displacement is taken as the product of the

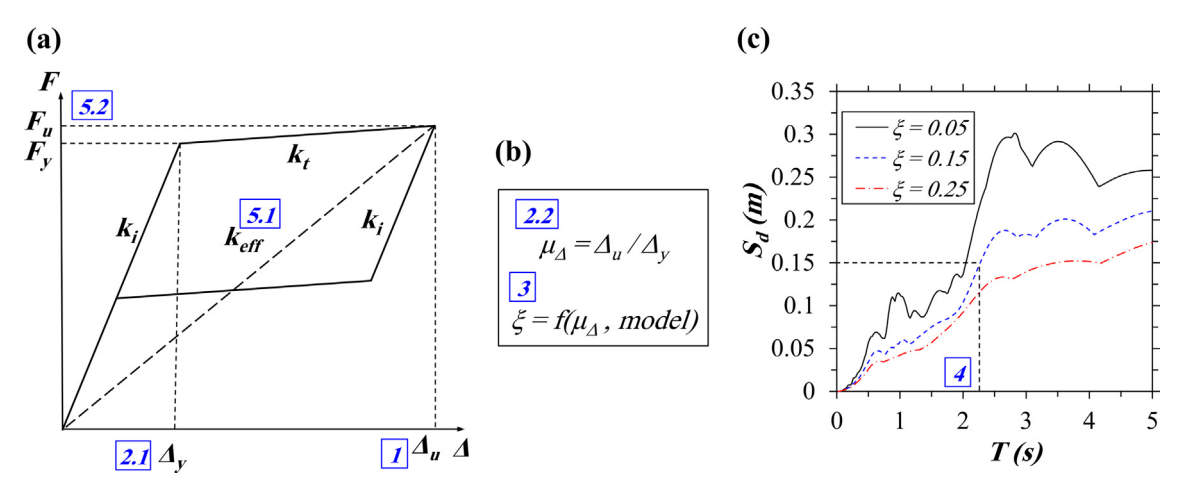


Fig. 3. Concept of equivalent viscous damping in DDBD method: (a) hysteretic response, (b) relation between  $\xi$  and  $\mu_{\Delta}$ , and (c) displacement response spectra for different values of  $\xi$ .

displacement of an equivalent linear elastic system, with the same initial damping ratio ( $\xi_e$ ) and initial lateral stiffness as the nonlinear system multiplied by a displacement modification factor. In the second approach, the maximum displacement is determined from a linear elastic system with a period shift (lower stiffness and higher structural period) and higher damping ratio than that the nonlinear system. In this study, the second approach was followed to determine  $\xi$  to estimate the maximum displacements. Evaluation of different methods and procedures to determine the EVD for various hysteresis models can be found in [28,29].

The concept of EVD for a structure was first presented by Jacobsen [26] to determine approximate solutions for nonlinear SDF systems with a damping force that is proportional to the nth power of the velocity. It is assumed that the two systems are under sinusoidal excitation, having the same stiffness and dissipating the same amount of energy each cycle. Jennings [30,31] modified Jacobsen's concept by changing the initial stiffness of the linear SDF system to a secant stiffness. The modified concept has been further investigated and extended by several researchers [29,32].

The modified Jacobsen's equivalent viscous damping ratio,  $\xi_J$ , for a nonlinear system with a hysteresis response comparable to a substitute linear system with secant stiffness can be estimated by modifying the original Jacobsen's model given in Eq. (2), where  $w_n$  is the natural vibration frequency of the system, and w is the loading vibration frequency.  $E_d$  represents the dissipated energy by the nonlinear system taken as  $2A_h$  (shown in Fig. 4) and  $E_s$  represents the stored energy by the substitute linear system taken as 0.5  $\Delta_u$   $F_u$  (see Fig. 4). Assuming that the loading frequency is similar to the system frequency  $(w_n/w=1)$  and substituting  $E_d$  and  $E_s$  results in the modified Jacobsen's equation for the equivalent viscous damping ratio as given in Eq. (3).

$$\xi_J = \frac{w_n}{4\pi w} \frac{E_d}{E_s} \tag{2}$$

$$\xi_J = \frac{A_h}{\pi F_u \Delta_u} \tag{3}$$

It should be mentioned that this equation ignores the conditions required for the two systems in the original Jacobsen's approach, which are as follows: (1) they are excited by sinusoidal loading, (2) they are at resonance conditions, and (3) they have the same stiffness.

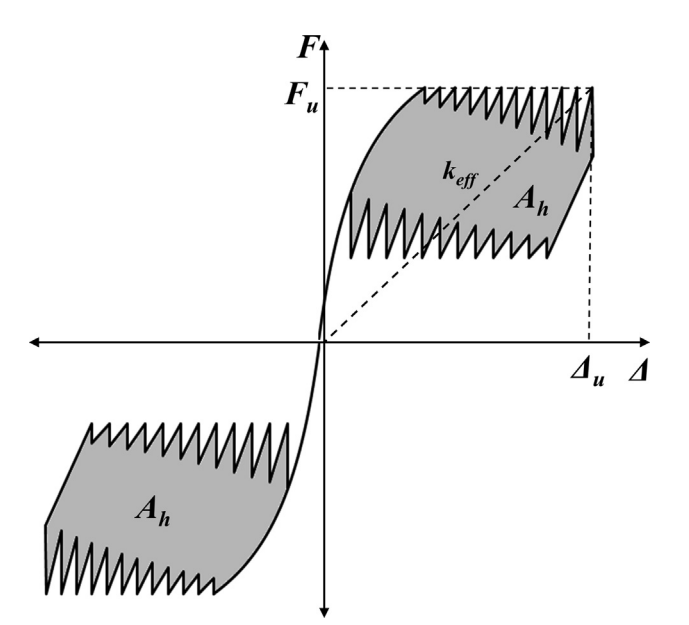


**Fig. 4.** Full cycle hysteretic response of the MCCD system with parameters for the modified Jacobsen's approach.

#### 2. Methods

## 2.1. Idealized hysteretic response of the MCCD system

To facilitate the nonlinear time-history analysis of structures incorporating the MCCD system, it is desired to idealize the hysteretic response. The reason is that the sawtooth-shape of the force–displacement, *F-∆*, curve (Fig. 4) imposes computational difficulties, and hence commonly used seismic structural analysis programs don't offer modeling tools to represent such a response. Thus, the response of the MCCD system was idealized to a flag-shaped (parallelogram) response by maintaining the energy balance between the actual and the idealized responses. This approach is similar to widely used approaches in the seismic design of structural elements to determine the ideal yield displacement (curvature, or rotation) [15,33].

The sawtooth-shape response of the MCCD system shown in Fig. 5(a) can be calculated using the analytical model presented in [12]. The study in [12] investigated the response characteristics of the MCCD system and its energy dissipation capability. As shown in Fig. 5(a), the response consists of multiple snap-through (and snap-back) events that equals the number of units in the system  $(n_s)$ . The snap-through and snap-back events are at the same level as the buckling force,  $F_b$ , and the minimum force,  $F_n$ , respectively. The drop forces from each snap-through,  $F_{bd}$ , and snap-back,  $F_{nd}$ , events vary depending on h/t and  $n_s$ . The effective initial stiffness of the system,  $k_b$ , is taken as the slope of a straight line from the origin to the displacement at the first buckling event,  $\Delta_b$ , of the system as given below:

$$k_b = F_b/\Delta_b \tag{4}$$

where  $\Delta_b = n_s \, \delta_b$ , and  $\delta_b$  is the critical (instability) displacement of an individual CCD unit as shown in Fig. 5(b). The response characteristics of a single CCD unit and its force and displacement values can be calculated using the expressions developed in [13]. The maximum displacement of the system,  $\Delta_m$ , is given as follows:

$$\Delta_m = n_s \delta_b + (n_s - 1) s_b \tag{5}$$

where  $s_b = \delta_b - \delta_m$ , and  $\delta_m$  is the displacement at a force level equal to  $F_b$  in Region III, see Fig. 5(b).

A two-step procedure was developed to idealize the hysteretic response of the MCCD system. In the first step, an ideal initial stiffness was determined in terms of h/t. This stiffness is needed to correct the initial stiffness  $(k_b)$  in order to construct a flag-shaped response that maintains the equal energy condition between the actual and idealized responses for a theoretical system with  $n_s = \infty$  (Fig. 6). In the second step, an ideal buckling force,  $F_b$ , and a minimum force,  $F_n$ , were determined based on the characteristics of the hysteretic response of the MCCD system. It should be noted that in practical systems with  $n_s \ll \infty$ ,  $F_b$  and  $F_n$  are smaller and greater than  $F_b$  and  $F_n$ , respectively. The values of  $F_b$  and  $F_n$  approach  $F_b$  and  $F_n$  respectively, when  $n_s$  approaches  $\infty$ .

## 2.1.1. Ideal stiffness

Fig. 6 shows the F- $\Delta$  response of an MCCD system with  $n_s = \infty$ . The F- $\Delta$  response of such as system is similar to the response of a single CCD under force control conditions. Note that in this case  $F_b' = F_b$  and  $F_n = F_n'$ . Fig. 6 also shows an idealized response based on the initial stiffness of the system  $(k_b)$ . This idealization clearly shows that the energy balance between the enclosed areas of the two curves is not maintained. Therefore, the initial stiffness of an idealized response,  $k_z$ , must be determined in a way that satisfies the energy balance condition. This can be done by solving the following equation for  $k_z$ :

$$A_h = (F_b - F_n)(\Delta_m - F_b/k_z) \tag{6}$$

Eq. (6) represents the area of the flag-shaped response and the ratio  $F_b / k_z$  represents the ideal displacement at first buckling event,  $\Delta_b'$ , see Fig. 6.

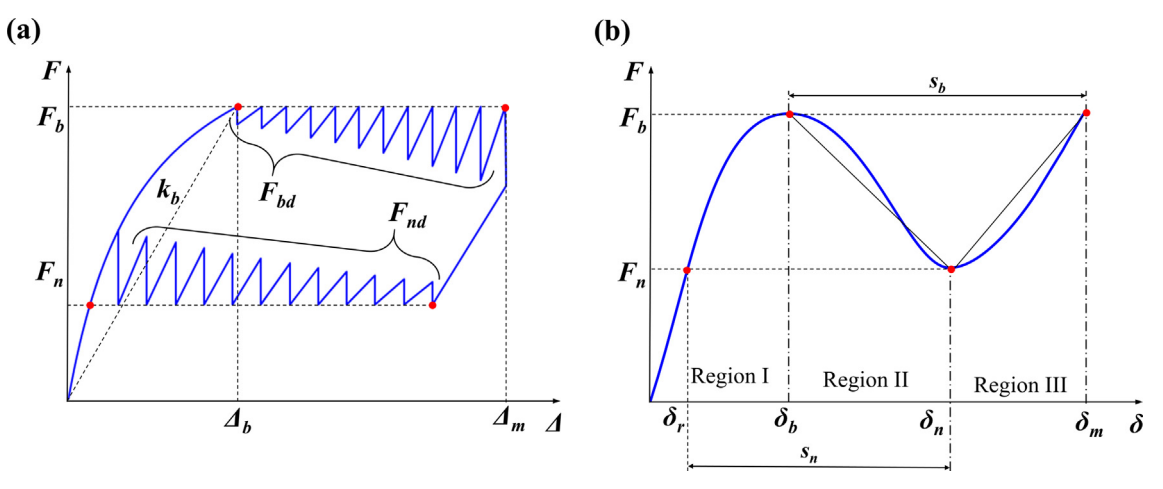


**Fig. 5.** (a) F- $\Delta$  response of the MCCD system, and (b) F- $\delta$  responses of a CCD unit with key response quantities.

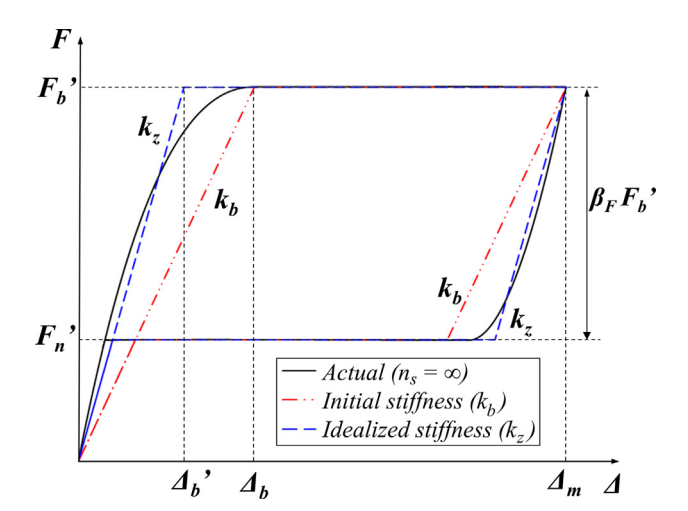


Fig. 6. The actual and the idealized F- $\Delta$  curves for an MCCD system with  $n_s=\infty$ 

Fig. 6 shows the ideal initial stiffness and the resulting hysteretic response of the system. The same process was conducted for h/t ranging from 1.5 to 3 in order to construct a relation between h/t and  $k_z/k_b$ . This relation was found to be linear as shown in Fig. 7(a). A linear regression analysis was conducted on the resulting data to develop a relationship

to calculate  $k_z/k_b$  over the considered h/t range as given in Eq. (7):

$$k_z/k_b = 0.674h/t \tag{7}$$

The equivalent viscous damping ratios based on the modified Jacobsen's approach  $(\xi_J)$  were calculated for h/t ranging from 1.5 to 3 using Eq. (3). The values of  $F_u$  and  $\Delta_u$  were taken as unity and  $\Delta_m/\Delta_b$ ', respectively. The results show an approximately linear relationship between  $\xi_J$  and h/t. Two more important quantities that describe the idealized hysteretic response are the displacement ductility  $(\mu_\Delta)$  and the force ratio of the difference between  $F_b$ ' and  $F_n$ ',  $\beta_F$  as given in Eqs. (8) and (9), respectively. The equations were used to construct a relation for  $\mu_\Delta$  and  $\beta_F$  with respect to h/t as shown in Fig. 7(b). Both quantities exhibit approximately linear relationships with h/t.

$$\mu_{\Delta} = \Delta_{\rm m} / \Delta_b^{'} \tag{8}$$

$$\beta_{F} = (F_{b}^{'} - F_{n}^{'})/F_{b}^{'} \tag{9}$$

## 2.1.2. Ideal maximum and minimum forces

For an MCCD system with a finite number of units  $(n_s \ll \infty)$ , the ideal buckling  $(F_b')$  and minimum  $(F_n')$  forces are lower and higher than  $F_b$  and  $F_n$ , respectively. Thus, the aim here is to determine the values of  $F_b'$  and  $F_n'$  in conjunction with the ideal initial stiffness  $(k_z)$ , determined in the first step, while maintaining the energy balance between the two responses as shown in Fig. 8. Since the known parameters of the idealized response in Fig. 8 are only  $k_z$  and  $\Delta_m$ , it is required to establish

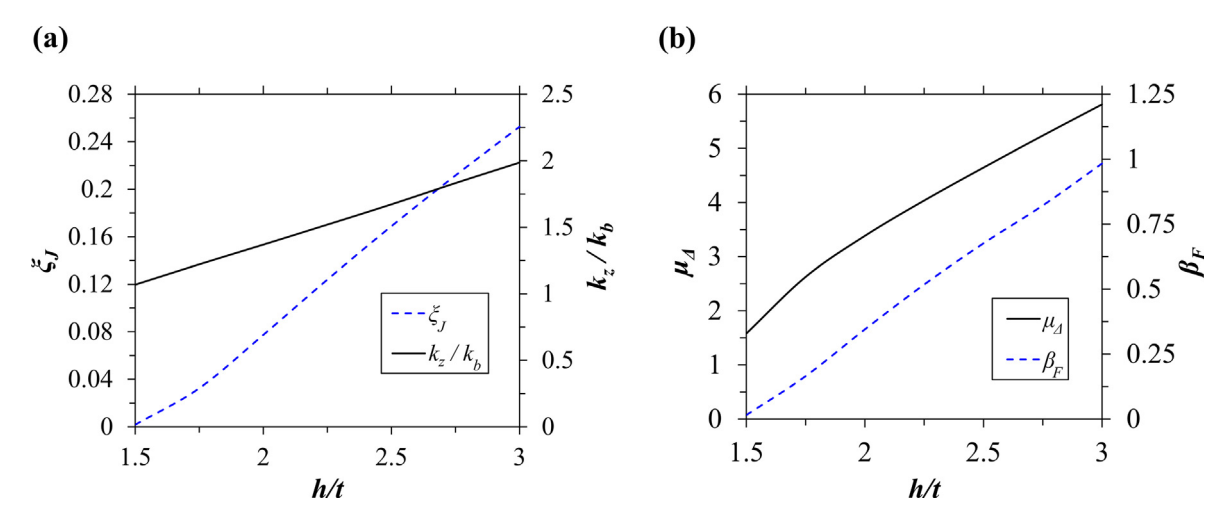
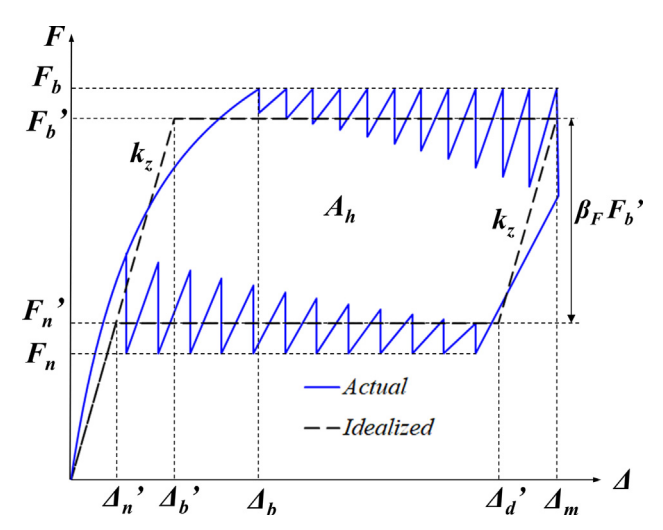


Fig. 7. (a) EVD ratios based on modified Jacobsen's approach  $(\xi_J)$  and the the ideal stiffness ratio  $(k_z/k_b)$  with h/t, and (b) displacement ductility  $(\mu_\Delta)$  and force difference ratio  $(\beta_F)$  with h/t.



**Fig. 8.** Actual and idealized  $F-\Delta$  curves for an MCCD system with  $n_s \ll \infty$ .

a relation between  $F_{b'}$  and  $F_{n'}$  in terms of the average buckling,  $F_{bavg}$ , and minimum,  $F_{nave}$ , forces to solve for the enclosed area equation  $A_h =$  $(F_b' - F_n')$   $(\Delta_m - F_b' / k_z)$  for  $F_b'$ . In this relation it is assumed that the difference between  $F_{b'}$  and  $F_{bavg}$  equals to the difference between  $F_{n'}$  and  $F_{navg}$ , i.e.,  $F_{b'} - F_{bavg} = F_{n'} - F_{navg}$ . This assumption ensures that the idealized forces are relative to the average forces, and that the reduction from  $F_b$  and the increase from  $F_n$  are equivalent to each other. The average forces  $F_{bavg}$  and  $F_{navg}$  can be calculated based on the average differences between  $F_b$  and  $F_{bd}$ , and between  $F_n$  and  $F_{nd}$ , see Fig. 5(a). The following steps summarize this idealization procedure:

- 1. Calculate the sawtooth-shaped response of the MCCD system and the energy area  $A_h$
- 2. Determine the average forces  $F_{bavg}$  and  $F_{navg}$
- 3. Solve the second-degree equation Eq. (10) of the enclosed energy area  $A_h$  and determine  $F_h$ ':

$$C_1 F_b^{'2} + C_2 F_b^{'} - C_3 = 0 {10}$$

 $C_1 = -2/k_z$ 

 $C_2 = 2\Delta_m + (F_{bavg} + F_{navg})/k_z$ , and

 $C_3 = \Delta_m(F_{bavg} + F_{navg}) + A_h$ 

- 4. Calculate  $F_n^{'}=F_{navg}-(F_b^{'}-F_{bavg})$ 5. Calculate  $\Delta_{b'}$ ,  $\Delta_{d'}$ , and  $\Delta_{n'}$  based on the value of  $F_{b'}$ ,  $F_{n'}$ , and  $k_z$  as shown in Fig. 8.

The procedure above was repeated for h/t ranging from 1.5 to 3 and for  $n_s$  ranging from 1 to 1000 to examine the relation of  $\mu_{\Delta}$  with  $n_s$  and h/t as shown in Fig. 9. It can be seen that in general the increase in  $\mu_{\Delta}$ with  $n_s$  is minimal especially for higher values of  $n_s$ . The reason is that both  $\Delta_m$  and  $\Delta_{h'}$  are in terms of  $n_s$ . Nonetheless,  $\mu_{\Delta}$  increases at higher rate for  $n_s$  between 3 and 6, and this effect is more pronounced for systems with higher h/t. However, as will be shown latter, the dissipated energy  $(A_h)$  within that range is low.

To study the relation between  $\xi_{J}$  and  $n_{s}$ , Eq. (3) was used to determine  $\xi_I$  for  $n_s = 1$  to 1000 and for h/t values ranging from 1.5 to 3. The values of  $F_u$  and  $\Delta_u$  were taken as unity and  $\Delta_m/\Delta_b$ , respectively. This relation is shown in Fig. 10(a). It should be noted that an MCCD system requires a h/t of about 1.5 to exhibit a snap-through instability and h/t of about 3 or less to maintain self-recoverability [12]. Fig. 10(a) shows that for  $n_s \le 2$ ,  $\xi_J = 0$  since the loading and unloading curves coincide, while for 2 <  $n_s \le 18$ ,  $\xi_J$  increases sharply. For about  $n_s > 18$ , a further increase in  $n_s$  results in a slight increase (< 10%) in  $\xi_J$ . Similarly, the force ratio  $\beta_F$  was plotted against h/t and  $n_s$  and it

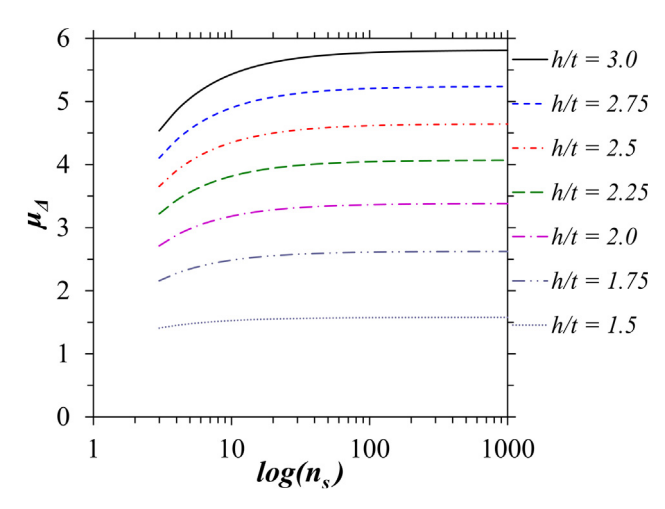


**Fig. 9.** The relation between displacement ductility  $(\mu_{\Delta})$  with  $n_s$  for a range of h/t values.

showed comparable trends to  $\xi_J$  as shown in Fig. 10(b).

#### 2.2. Considered cases for the study

Two cases of the hysteresis model were considered for the study: (1) the response of the MCCD system, and (2) the response of the MCCD system coupled with a linear elastic response. In the first case, it is assumed that the MCCD is the only force resisting system and damping mechanism with a response as shown in Fig. 11(a). Note that the tangent stiffness,  $k_t$ , is zero in this case. In the second case, the response in the first case (i.e., the response of the MCCD system) is coupled in parallel with a non-yielding linear (NYL) system. The resulting response in the second case is as shown in Fig. 11(b). The coupled NYL system has a stiffness,  $k_c$ , that is less than or equal to the secant stiffness of the MCCD system,  $k_e$ , as shown Fig. 11(b). The ultimate force of the NYL system,  $F_c$ , can be linked to  $F_b$  by the force ratio factor,  $\gamma_F$ , as given below.  $\gamma_F = 1$  and 2 for  $F_c = 0$  and  $F_c = F_b'$ , respectively. It is should be noted that  $k_{eff}$  in the first case [Fig. 11(a)] does not equal to  $k_{eff}$  in the second case [Fig. 11(b)]. The relations governing the parameters of hysteretic responses are as follows:

$$\gamma_F = (F_b^{'} + F_c)/F_b^{'} \tag{11}$$

$$F_u = k_{eff} \Delta_u \tag{12}$$

$$F_{y} = F_{u} \frac{\mu_{\Delta} + \gamma_{F} - 1}{\gamma_{F} \mu_{\Delta}} \tag{13}$$

$$k_i = F_{\nu} \mu_{\Lambda} / \Delta_{\rm u} \tag{14}$$

$$\alpha_F = \frac{\gamma_F - 1}{\mu_\Delta + \gamma_F - 1} \tag{15}$$

$$k_t = \alpha_F k_i \tag{16}$$

$$\xi_J = \frac{\beta_F (\mu_\Delta - 1)}{\gamma_F \pi \mu_\Delta} \tag{17}$$

## 2.3. Ground motion records

A set of 62 ground motion records from 7 different earthquakes (see Table 1) were used in this study. The earthquakes had magnitudes (Ms) ranging from 5.8 to 7.1 [34]. The records were recorded on sites corresponding to site class B as per [35]. Fig. 12 shows the displacement response spectra for the 62 ground motion records with 5% damping along with the average response spectrum. The curves in Fig. 12 were normalized based on maximum spectral displacement after the spectral

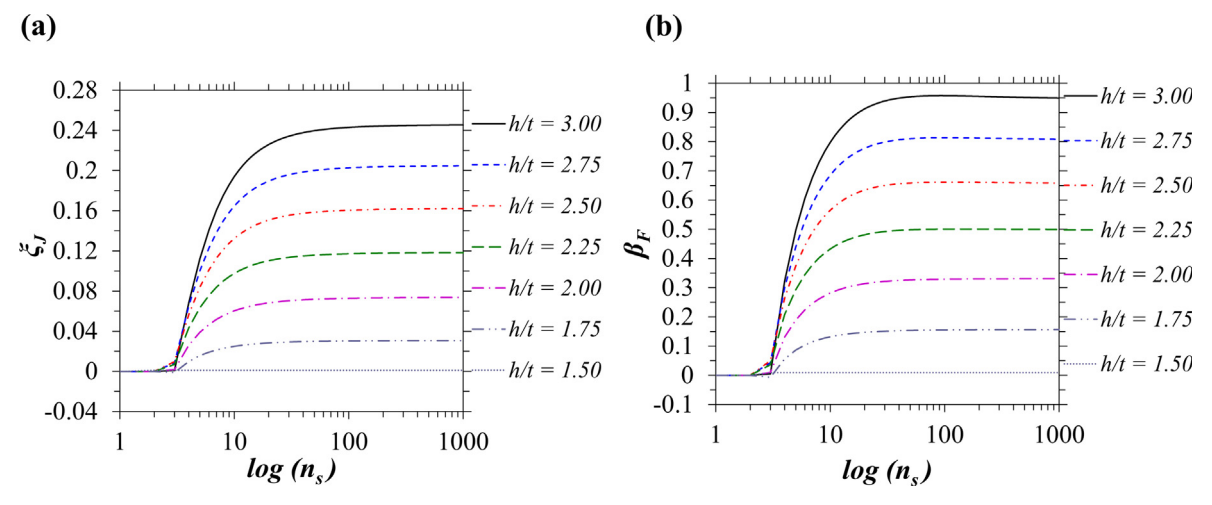


Fig. 10. (a) The relation between  $\xi_J$  with  $n_s$  for different h/t ratios, and (b)  $\beta_F$  with h/t for different  $n_s$  values.

analysis for illustration purposes. The response characteristics of the individual responses and their averaged response in Fig. 12 are important to compare the used ground motion records with design response spectra.

## 2.4. Analysis procedure

The procedure followed to determine the  $\xi$  starts with the modified Jacobsen's viscous damping ratio  $(\xi_J)$  defined by Eq. (3) in addition to the elastic viscous damping  $(\xi_e)$  of 2% as an initial estimate for the linear THA of the substitute systems. These ratios are then changed in an iterative process until the resulting  $\xi$  for the equivalent substitute linear SDF systems have the same maximum spectral displacements as the original nonlinear systems. For the nonlinear THA, a value of 2% Rayleigh damping [36–38] proportional to the current tangent stiffness was considered.

The study was conducted for the two cases noted in Section 2.2 with  $T_{eff}$  ranging from 0.05 to 4 s at 0.05 s increments and 1.5  $\leq h/t \leq$  3 at 0.25 increments. The corresponding values of  $\mu_A$  and  $\beta_F$  as a function of

Table 1
Recorded earthquake used in this study.

Date	Earthquake name	Magnitude (Ms)
02/09/1971	San Fernando	6.5
04/24/1984	Morgan Hill	6.1
07/08/1986	Palm Springs	6.0
10/01/1987	Whittier	6.1
10/17/1989	Loma Prieta	7.1
06/28/1991	Sierra Madre	5.8
01/17/1994	Northridge	6.8

h/t are shown in Fig. 7(b) and can be calculated using Eqs. (8) and (9), respectively.

The THA of the linear and nonlinear systems were performed using the program Opensees [39]. The iterative process to determine  $\xi$  for the linear SDF systems were performed using the program Matlab. The process to determine the EVD ratios is as follows:

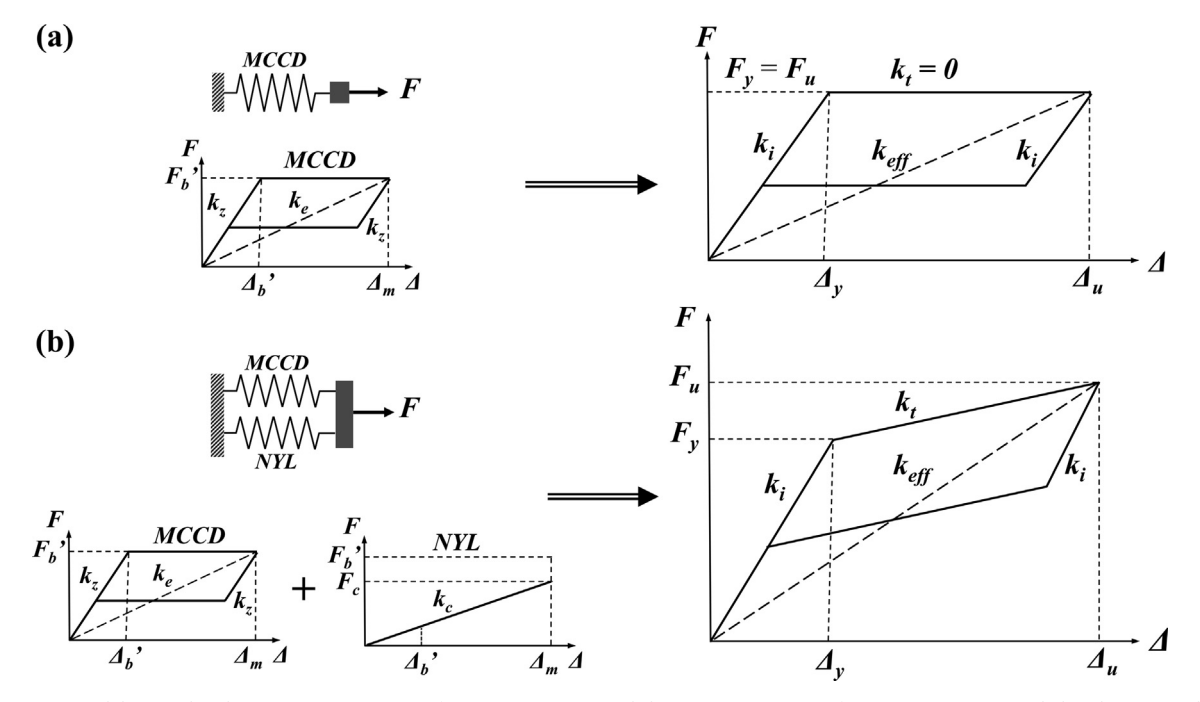
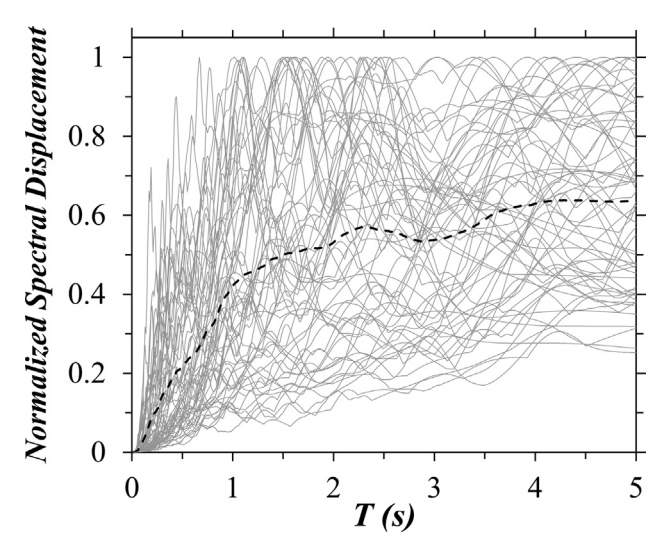


Fig. 11. Hysteresis models considered: (a) Case 1 - response of an MCCD system, and (b) Case 2 - response of an MCCD system coupled with a non-yielding linear system.



**Fig. 12.** Scaled displacement response spectra of the motion records at 5% damping and their average response.

- 1. Set an h/t and calculate the corresponding values of  $\mu_{\Delta}$  and  $\beta_{F}$ .
- 2. Select a ground motion record.
- 3. Set an effective structural period  $T_{eff}$ .
- 4. Calculate  $\xi_J$  from Eq. (3) and set the initial EVD ratio,  $\xi_i$ , as  $\xi_i = \xi_e + \xi_J$ .

- 5. Calculate  $k_{eff} = 4 \pi^2 m / T_{eff}^2$  where m is the mass and it was kept constant at unity.
- 6. Perform linear THA on the SDF system with properties as given above and determine the maximum absolute linear displacement,  $\Delta_I$ .
- 7. Based on the value of  $\Delta_L$  from step 6, and  $\mu_\Delta$  and  $\beta_F$  form step 1, calculate the parameters of the hysteretic response of the nonlinear system:  $F_{tv}$ ,  $F_{vv}$ ,  $k_{tv}$ , and  $k_t$  using the relations presented in Section 2.2.
- 8. Perform nonlinear THA on the SDF system with properties as given above and determine the maximum absolute nonlinear displacement. Ass...
- 9. Compare the maximum displacements  $\Delta_L$  and  $\Delta_{NL}$  from steps 6 and 8, respectively, and report the ratio  $\Delta_{NL}/\Delta_L$ . If the error between  $\Delta_L$  and  $\Delta_{NL}$  is < 1.5%, then the EVD ratio  $\xi$  equals  $\xi_i$  and proceed to step 11, otherwise proceed to step 10.
- 10. For the linear system with properties as given in steps 2 to 5, iteratively change  $\xi$  until the resulting new  $\Delta_L$  equals to  $\Delta_{NL}$  from step 8 within an absolute error of 1.5%, and report the results.
- 11. Repeat the procedure from step 3 to 10 by selecting different values of  $T_{eff}$ . This step will result in linear and nonlinear displacement response spectra.
- Repeat the procedure from step 2 to 11 by selecting another ground motion record.
- 13. Repeat the procedure from step 1 to 12 by selecting a different value of h/t and the corresponding values of  $\mu_{\Delta}$  and  $\beta_F$ .

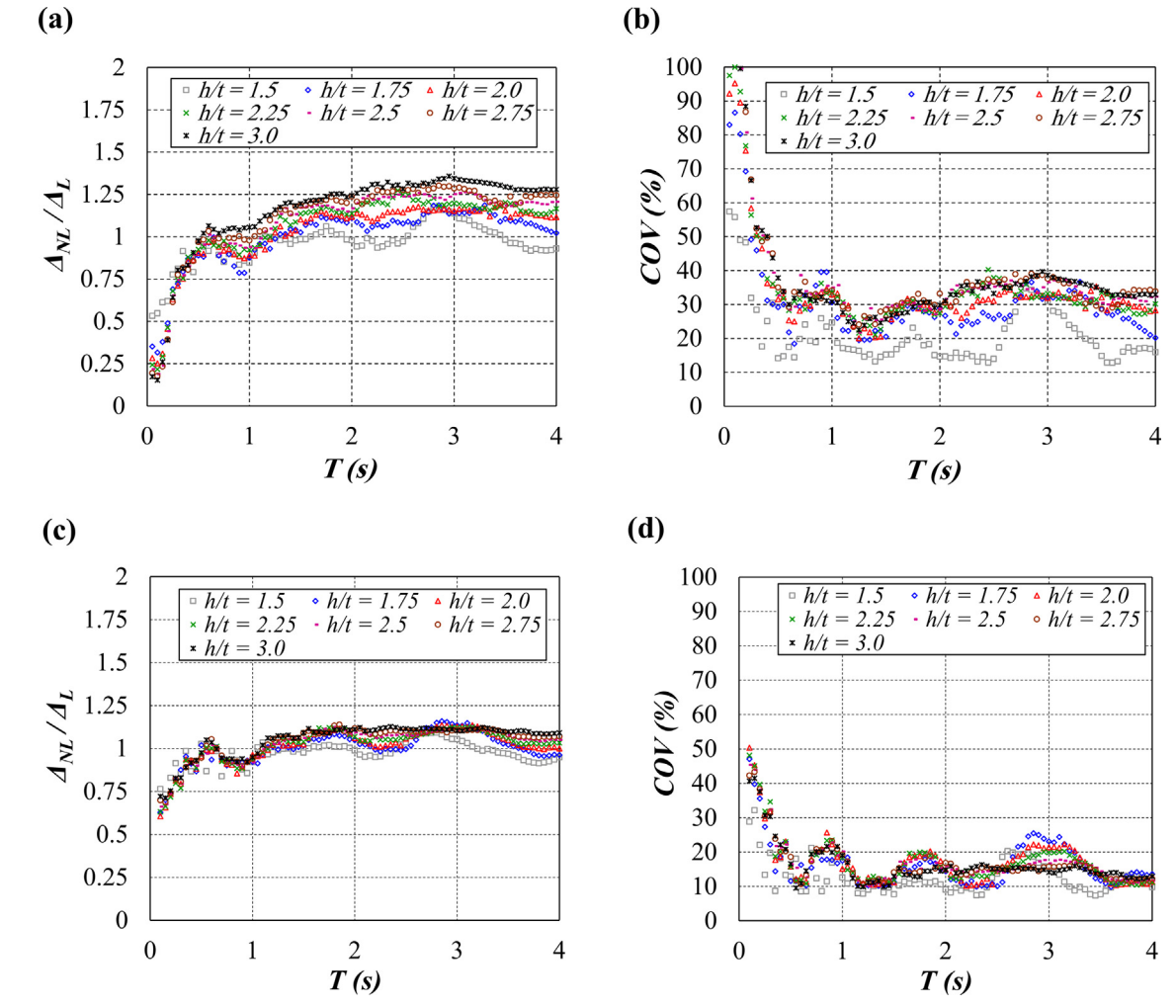


Fig. 13. Average ratios of linear to nonlinear spectral displacements and coefficient of variation for Case 1 [(a) and (b)], and for Case 2 [(c) and (d)].

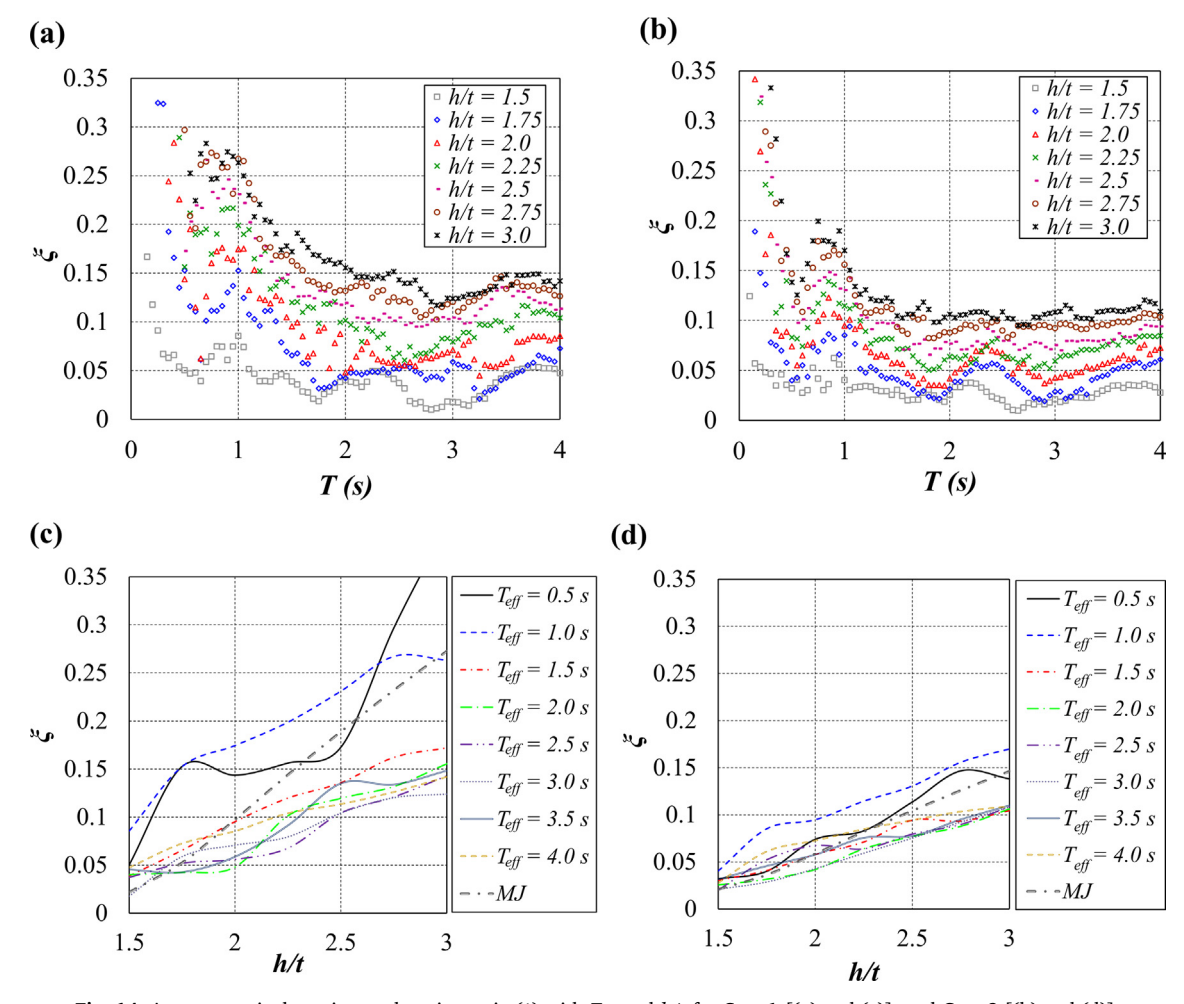


Fig. 14. Average equivalent viscous damping ratio  $(\xi)$  with  $T_{eff}$  and h/t for Case 1 [(a) and (c)], and Case 2 [(b) and (d)].

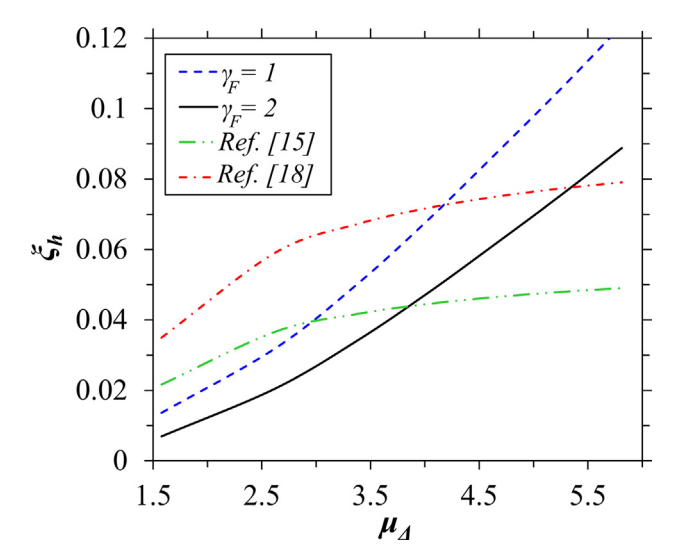


Fig. 15. Developed expression for EVD compared with other expressions.

## 3. Results and discussion

## 3.1. Ratio of nonlinear to linear spectral displacements

The linear and nonlinear spectral displacements (analysis results from step 11) for the considered ground motion records were averaged and grouped based on the h/t values and the two considered cases in

Section 2.2. The calculated ratios of nonlinear to linear spectral displacements  $(\Delta_{NL}/\Delta_L)$  were averaged for the 62 records over the range of  $T_{eff}$ . A statistical study was conducted on the resulting data to determine the upper and lower bounds using the interquartile range [40] and then eliminating suspected outliers. Fig. 13(a) and (c) show the averaged ratios of  $\Delta_{NL}/\Delta_L$  for Cases 1 and 2, respectively. It can be noted that for approximately  $T_{eff}>0.75$  s, the ratio is generally > 1. This means that the used  $\xi_i$  based on the modified Jacobsen's approach (step 4) overestimates  $\xi$ . An opposite conclusion can be made on the  $\Delta_{NL}/\Delta_L$  values for  $T_{eff}<0.75$  s. The coefficient of variation (COV) for  $T_{eff}<0.75$  s, shown in Fig. 13(b) and (d), ranges between 10% and 40% for Case 1, and between 8% and 28% for Case 2.

## 3.2. Equivalent viscous damping ratios

A similar statistical study to that performed for the  $\Delta_{NL}/\Delta_L$  ratios was repeated for the equivalent viscous damping ratio ( $\xi$ ) obtained from the iterative process in step 10. Fig. 14(a) and (b) show the average  $\xi$  for the 62 records over the range of  $T_{eff}$  and grouped based on the values of h/t and the two considered cases. Fig. 14(c) and (d) show the relation between h/t and  $\xi$  for selected values of  $T_{eff}$  along with the calculated EVD based on the modified Jacobsen's approach (MJ). The figures show that the curves are generally lower than the MJ curve except for shorter periods  $T_{eff}$ .

## 3.3. Developed expressions for equivalent viscous damping

The resulting equivalent viscous damping ratios from the analysis

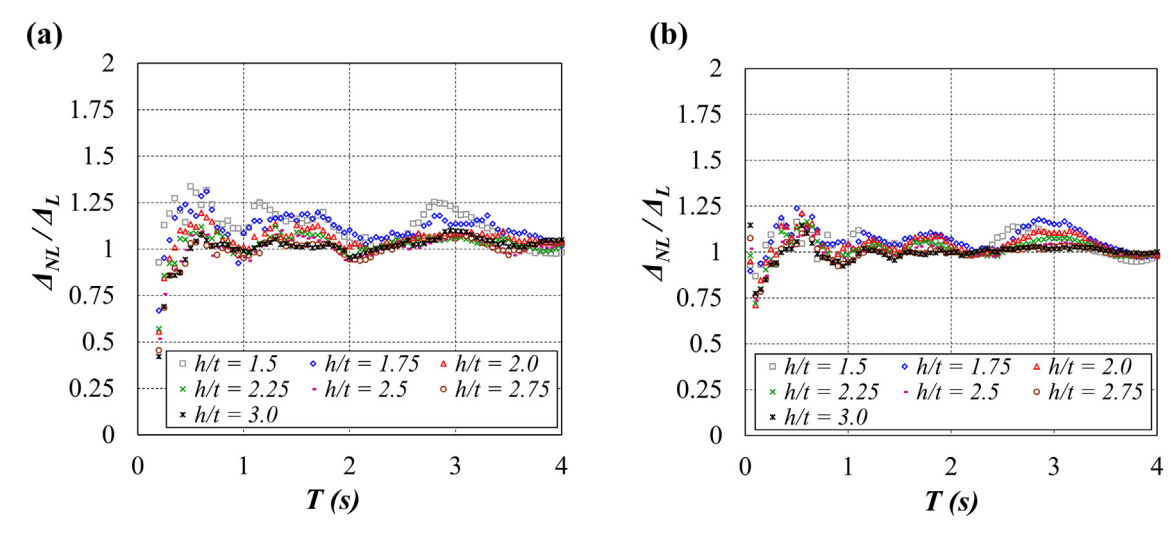


Fig. 16. Averaged ratio of linear to nonlinear spectral displacements using the developed expressions for (a) Case 1, and (b) Case 2.

procedure (Fig. 14) were used to develop empirical expressions for EVD ratios  $(\xi_h)$  of the idealized hysteretic responses of MCCD systems [see Eq. (1)]. The data are mainly influenced by height-to-thickness ratio (h/t), the effective structural period  $(T_{eff})$ , and the force factor of the coupled NYL system  $(\gamma_F)$ . A piecewise linear function was used to develop an expression for  $\xi_h$  as given by Eqs. (18)–(21). The function consists of constant and linear parts that meet at a deviation point,  $T_s$ , along the range of structural period. This point was found to be a function of  $\gamma_F$ . The ideal height-to-thickness ratio,  $(h/t)_n$ , can be calculated using Eq. (22) based on the values of  $\mu_\Delta$  and  $\beta_F$  of the considered system. For systems with  $n_s = \infty$ ,  $(h/t)_n = h/t$ , while for systems with  $n_s \ll \infty$ ,  $(h/t)_n < h/t$ .

$$\xi_h = D[1 + E(T_s - T_{eff})] \quad \text{for} \quad T_{eff} < T_s$$
 (18a)

$$\xi_h = D \quad \text{for} \quad T_{eff} < T_{s}$$
 (18b)

$$T_s = -0.5\gamma_F + 2.5 \tag{19}$$

$$D = (-0.0188\gamma_F + 0.0922)(h/t)_n + 0.0215\gamma_F - 0.1188$$
 (20)

$$E = 3.817(h/t)_n^{-1.422} (21)$$

$$(h/t)_n = 0.183\mu_{\Delta} + 0.768\beta_F + 1.151 \tag{22}$$

The developed expression in Eq. (18) was compared to the expressions proposed in [15,18] to estimate  $\xi_h$  for ring-spring dampers, which have a flag shaped response. Since the ratio h/t does not apply to the expressions in [15,18], the corresponding  $\mu_{\Delta}$  values to the h/t ratios in the developed model were set as the basis for the comparison. Fig. 15 shows the relation between  $\xi_h$  and  $\mu_\Delta$  for  $\gamma_F$  of 1 and 2. The figure illustrates the difference in dealing with the MCCD system compared to conventional ring-spring dampers as well as inelastic (ductile) systems. It can be seen that at higher values of  $\mu_{\Delta}$  the  $\xi_h$  based on the expressions in [15,18] reach a plateau, which means that the width of the hysteretic response doesn't significantly increase with increasing deformations. On the other hand, the  $\xi_h$  of the MCCD system using the developed expression in Eq. (18) keeps increasing. This agrees with the trends shown in Fig. 14(c) and (d). The reason is that increasing  $\mu_{\Delta}$  results in increasing h/t which in turn increases the force difference factor  $(\beta_F)$ and hence the area of the hysteretic envelope, or dissipated energy. This is shown in Figs. 7 and 10.

The linear substitute systems were reanalyzed with damping ratios estimated by the developed expressions. The linear and nonlinear spectral displacements for the used ground motion records were averaged and grouped based on the values of h/t for the considered cases. Results are shown in Fig. 16, from which can be seen that the spectral displacements are in good agreement.

## 3.4. Illustrative example

The equivalent viscous damping ratio is estimated for an MCCD system with  $n_s=12$ , h/t=2.5, and CCD units with thickness, height, and length of 1.2 mm, 3 mm, 100 mm, respectively. The MCCD system is coupled with an NYL system with a force ratio factor  $\gamma_F=1.649$ . The -F- $\Delta$  response of the MCCD system was calculated using the multilinear model presented in [12]. The idealized hysteretic response of the MCCD system was also calculated using the procedure presented in Section 2.1. From the idealized response the following factors can be calculated assuming  $T_{eff} > T_s$  as:

$$\beta_F = (F_b^{'} - F_n^{'})/F_b^{'} = 0.5586$$

$$\mu_{\Delta} = \Delta_m/\Delta_b' = 4.6676$$

$$(h/t)_n = 0.183\mu_{\Delta} + 0.768\beta_F + 1.151 = 2.4341$$

$$D = (-0.0188\gamma_F + 0.0922)(h/t)_n + 0.0215\gamma_F - 0.1188 = 0.0656$$

$$\xi_h = D = 0.0656$$

The estimated  $\xi_h$  for the system is about 6.5%. In case where the calculated  $T_{eff}$  (using the DDBD method presented in Section 1.2) is smaller than  $T_s$ , the factor E in Eq. (21) must be calculated and Eq. (18a) must be used to calculate  $\xi_h$ .

#### 4. Conclusions

The hysteretic response of an MCCD system that relies on consecutive snap-through buckling events to dissipate energy was investigated for its equivalent viscous damping. The sawtooth-shape response of the MCCD system was idealized to facilitate dynamic analysis. The idealization process was based on maintaining energy balance between the original and idealized responses.

The modified Jacobsen's approach was used to initiate the process of determining equivalent viscous damping ratios for the examined hysteretic model. The approach is based on substituting the nonlinear system by a linear system with a secant stiffness at maximum displacement, which agrees with the basic assumptions of the direct displacement-based design method.

Linear and nonlinear time-history analyses were performed on single degree of freedom systems with hysteretic response and linear equivalents, and a systematic analysis procedure was followed to determine corrected equivalent viscous damping ratios for the examined responses. A statistical study was conducted to develop empirical expressions for the idealized hysteretic response of the MCCD system. The

following findings were drawn from the study:

- 1. Ratios of nonlinear to linear spectral displacement show that the equivalent viscous damping ratios based on the modified Jacobsen's approach are overestimated. This behavior is more pronounced in intermediate and long period ranges ( $T_{eff} > 0.75$  s). The opposite behavior was observed in the short period range ( $T_{eff} < 0.75$  s).
- 2. The general coefficients of variation of nonlinear to linear spectral displacements were 23% and 11% for Cases 1 and 2, respectively.
- 3. An expression to estimate the hysteretic equivalent viscous damping ratio was developed. The calculated spectral displacements for the linear substitute structure using the developed expression are in good agreement with displacements from the analyses of nonlinear systems.
- 4. An experimental investigation is being carried out to determine the EVD ratio of the MCCD system for a range of h/t values. Preliminary results show good agreement with the numerical results of this work.

#### CRediT authorship contribution statement

**Mansour Alturki:** Conceptualization, Methodology, Writing - original draft. **Rigoberto Burgueño:** Conceptualization, Supervision, Writing - review & editing.

#### **Declaration of Competing Interest**

The authors declare that they have no known competing financial interests or personal relationships that could have appeared to influence the work reported in this paper.

## Acknowledgement

The presented work was carried out with partial support from the U.S. National Science Foundation under grant number CMMI-1762119.

#### References

- [1] Frenzel T, Findeisen C, Kadic M, Gumbsch P, Wegener M. Tailored buckling mcrolattices as reusable light-weight shock absorbers. Adv Mater 2016;28:5865–70. https://doi.org/10.1002/adma.201600610.
- [2] Restrepo D, Mankame ND, Zavattieri PD. Phase transforming cellular materials. Extrem Mech Lett 2015;4:52–60. https://doi.org/10.1016/j.eml.2015.08.001.
- [3] Izard AG, Alfonso RF, McKnight G, Valdevit L. Optimal design of a cellular material encompassing negative stiffness elements for unique combinations of stiffness and elastic hysteresis. Mater Des 2017;135:37–50. https://doi.org/10.1016/j.matdes. 2017.09.001.
- [4] Correa DM, Klatt T, Cortes S, Haberman M, Kovar D, Seepersad C. Negative stiffness honeycombs for recoverable shock isolation. Rapid Prototyp J 2015;21:193–200. https://doi.org/10.1108/RPJ-12-2014-0182.
- [5] Shan S, Kang SH, Raney JR, Wang P, Fang L, Candido F, et al. Multistable architected materials for trapping elastic strain energy. Adv Mater 2015;27:4296–301. https://doi.org/10.1002/adma.201501708.
- [6] Liu S. Harnessing elastic instabilities for energy transduction, Doctoral dissertation. Michigan State University; 2019.
- [7] Ha CS, Lakes RS, Plesha ME. Design, fabrication, and analysis of lattice exhibiting energy absorption via snap-through behavior. Mater Des 2018;141:426–37. https:// doi.org/10.1016/j.matdes.2017.12.050.
- [8] Hu N, Burgueño R. Buckling-induced smart applications: recent advances and trends. Smart Mater Struct 2015;24:063001https://doi.org/10.1088/0964-1726/ 24/6/063001.
- [9] Liu S, Azad AI, Burgueño R. Architected materials for tailorable shear behavior with energy dissipation. Extrem Mech Lett 2019;28:1–7. https://doi.org/10.1016/j.eml. 2019.01.010.
- [10] Symans MD, Charney FA, Whittaker AS, Constantinou MC, Kircher CA, Johnson

- MW, et al. Energy dissipation systems for seismic applications: current practice and recent developments. J Struct Eng 2008;134:3–21.
- [11] Constantinou MC, Soong TT, Dargush GF. Passive energy dissipation systems for structural design and retrofit. Buffalo, NY: Multidisciplinary Center for Earthquake Engineering Research; 1998.
- [12] Alturki M, Burgueño R. Multistable cosine-curved dome system for elastic energy dissipation. J Appl Mech 2019;86:091002https://doi.org/10.1115/1.4043792.
- [13] Alturki M, Burgueño R. Response characterization of multistable shallow domes with cosine-curved profile. Thin-Walled Struct 2019;140:74–84. https://doi.org/ 10.1016/j.tws.2019.03.035.
- [14] Priestley MJN. Performance based seismic design. In: 12th World Conf. Earthq. Eng., New Zealand Society for Earthquake Engineering, Upper Hutt, New Zealand, 2000. p. 2831.
- [15] Priestley MJN, Calvi GM, Kowalsky MJ. Displacement-based seismic design of structures. Pavia, Italy: IUSS Press; 2007.
- [16] Priestley MJN, Grant DN. Viscous damping in seismic design and analysis. J Earthq Eng 2005;9:229–55. https://doi.org/10.1142/S1363246905002365.
- [17] Khan E, Kowalsky MJ, Nau JM. Equivalent viscous damping model for short period reinforced concrete bridges. J Bridg Eng 2016;21:04015047. https://doi.org/10. 1061/(ASCE)BE.1943-5592.0000803.
- [18] Dwairi HM, Kowalsky MJ, Nau JM. Equivalent damping in support of direct displacement-based design. J Earthq Eng 2007;11:512–30. https://doi.org/10.1080/ 13632460601033884
- [19] Blandon CA, Priestley MJN. Equivalent viscous damping equations for direct displacement based design. J Earthq Eng 2005;9:257–78. https://doi.org/10.1142/S1363246905002390.
- [20] Pennucci D, Sullivan TJ, Calvi GM. Displacement reduction factors for the design of medium and long period structures. J Earthq Eng 2011;15:1–29. https://doi.org/ 10.1080/13632469.2011.562073.
- [21] Xia Y, Wu Z, Kang Z, Li C. Stochastic response characteristic and equivalent damping of weak nonlinear energy dissipation system under biaxial earthquake action. Math Probl Eng 2017. https://doi.org/10.1155/2017/7384940.
- [22] Liu T, Briseghella B, Zhang Q, Zordan T. Equivalent damping of bilinear hysteretic SDOF system considering the influence of initial elastic damping. Soil Dyn Earthq Eng 2017;97:74–85. https://doi.org/10.1016/j.soildyn.2017.01.017.
- [23] Chopra AK. Dynamics of structures: theory and applications to earthquake engineering. 4th ed. Upper Saddle River, NJ: Prentice Hall; 2012.
- [24] Meirovitch L. Fundamentals of vibrations. Long Grove, IL: Waveland Press; 2001.
- [25] Weber F, Maślanka M. Precise stiffness and damping emulation with MR dampers and its application to semi-active tuned mass dampers of Wolgograd Bridge. Smart Mater Struct 2014;23:015019https://doi.org/10.1088/0964-1726/23/1/015019.
- [26] Jacobsen LS. Steady forced vibration as influenced by damping. Trans Am Soc Mech Eng 1930;52:169–81.
- [27] Papagiannopoulos GA. Jacobsen's equivalent damping concept revisited. Soil Dyn Earthq Eng 2018. https://doi.org/10.1016/j.soildyn.2018.08.001.
- [28] Miranda E, Ruiz-Garca J. Evaluation of approximate methods to estimate maximum inelastic displacement demands. Earthq Eng Struct Dyn 2002;31:539–60. https:// doi.org/10.1002/eqe.143.
- [29] Hadjian AH. A re-evaluation of equivalent linear models for simple yielding systems. Earthq Eng Struct Dyn 1982;10:759–67. https://doi.org/10.1002/eqe. 4290100602
- [30] Jennings PC. Periodic response of a general yielding structure. J Eng Mech Div 1964;90:131-66.
- [31] Jennings PC. Equivalent viscous vamping for yielding structures. J Eng Mech Div 1968;94:103–16.
- [32] Iwan WD, Gates NC. The effective period and damping of a class of hysteretic structures. Earthq Eng Struct Dyn 1979;7:199–211. https://doi.org/10.1002/eqe. 4290070302.
- [33] Paulay T, Priestley MJN. Seismic design of reinforced concrete and masonry buildings. New York, NY: Wiley & Sons; 1992.
- [34] Miranda E. Inelastic displacement ratios for structures on firm sites. J Struct Eng 2000;126:1150–9.
- [35] Federal emergency management agency, improvement of nonlinear static seismic analysis procedures, Washington, D.C., 2005.
- [36] Hall JF. Problems encountered from the use (or misuse) of Rayleigh damping. Earthq Eng Struct Dyn 2006;35:525–45. https://doi.org/10.1002/eqe.541.
- [37] Charney FA. Unintended consequences of modeling damping in structures. J Struct Eng 2008;134:581–92. https://doi.org/10.1061/(ASCE)0733-9445(2008) 134:4(581).
- [38] Petrini L, Maggi C, Priestley MJN, Calvi GM. Experimental verification of viscous damping modeling for inelastic time history analyzes. J Earthq Eng 2008;12:125–45. https://doi.org/10.1080/13632460801925822.
- [39] Mazzoni GL, McKenna S, Scott F, MH, & Fenves, OpenSees command language manual; 2006.
- [40] Moore DS, McCable GP, Craig BA. Introduction to the practice of statistics. 6th ed. New York, NY: W.H. Freeman; 2009.